Residual Stress in Cr$_{99}$Al$_1$ Polycrystalline Thin Films

Z.P. Mudau^a, C.J. Sheppard^{a*}, A.R.E. Prinsloo^a, A.M. Venter^b, T.P. Ntsoane^b
and E.E. Fullerton^c

^{a}Cr Research Group, Department of Physics, University of Johannesburg, Auckland Park, RSA
^{b}Research and Development Division, Necsa, Pretoria, RSA
^{c}Center for Memory and Recording Research, University of California San Diego, La Jolla, CA, 92093-0401 USA

The magnetic phase diagram of bulk Cr$_{100-x}$Al$_x$ shows interesting behaviour close to the triple point concentration of $x \approx 2$. Since the magnetic properties of Cr are influenced by dimensionality, stress and strain, this study focussed on the investigation of Cr$_{99}$Al$_1$ thin films prepared on fused silica substrates with thicknesses t varying from 29 to 452 nm using sputtering techniques. Resistance measurements covering the temperature range 2 to 400 K did not show any clear anomalies that could be indicative of changes in the magnetic ordering. X-ray diffraction (XRD) and atomic force microscopy (AFM) studies indicate the films are polycrystalline textured and that the 80 nm sample has the smallest grain size. In-plane stresses in these thin films were studied using the specialised XRD $\sin^2 \psi$-method. The results show that the stress varies with film thickness. The 29 nm sample has stress in the order of 833 MPa and with increasing film thickness the stress reaches 1471 MPa for the 80 nm layer, where after it systematically reduces for the thicker coatings to 925 MPa for the 452 nm film. The highest stress for the Cr$_{99}$Al$_1$ thickness sample series is seen in the film with the smallest grain size.

1. Introduction

Cr and its alloys exhibit a richness of magnetic phenomena that is directly linked with their spin-density-wave (SDW) antiferromagnetism [1]. The Néel transition temperature (T_N) of bulk Cr is strongly influenced by a variety of factors including doping, dimensionality, pressure and strain, making it an ideal material for the tailoring of specific, desired properties [1, 2].

Doping Cr with Al results in an interesting magnetic phase diagram for bulk Cr$_{100-x}$Al$_x$, that reveals the co-existence of the commensurate (C) SDW, incommensurate (I) SDW and paramagnetic (P) phases at $x \approx 2$ [1]. It is also known that thin films and heterostructures of Cr and its alloys have fascinating properties, not observed in the bulk, including proximity induced magnetic effects, the mediating role of Cr films in exchange coupled superlattices and in giant magnetoresistive (GMR) materials [2]. Combining these aspects, the present study extends research of the Cr$_{100-x}$Al$_x$ system to probe the physical properties in Cr$_{99}$Al$_1$ thin films of various thicknesses t, deposited on fused silica substrates. Resistance measurements on the films [3] in the temperature range 2 to 400 K did not show any clear anomalies reminiscent of changes in magnetic ordering. It is assumed that the T_N-values in this system have been driven higher due to stress effects [3] and that the T_N-values exceed 400 K. The latter contributions are probed in the present investigation.

Residual stress in thin films results from a variety of factors [4, 5]. Strain is an intrinsic materials parameter that can be measured by various techniques [6]. As diffraction based investigations are non-destructive and directly measures the spacing between atomic planes as a built-in material strain gauge [7], this is the first option to consider. The strains in the thin films were therefore determined using the XRD $\sin^2 \psi$-technique introduced by Noyen *et al.* [4] and discussed in full by Mudau *et al.* [8]. This method is a differential technique which then does not require standard references for calibration of the stress-free lattice spacing [9] and was also used to determine the strain in Cr thin films [8].

In this paper results are reported on the stress in a series of Cr$_{99}$Al$_1$ thin films of varying t, deposited on fused silica substrates, as obtained from XRD measurements.

2. Experimental method

The Cr$_{99}$Al$_1$ films with 29 nm $\leqslant t \leqslant$ 452 nm were prepared as described previously [3]. XRD measurements were done on a Bruker D8 Discover diffractometer equipped with a Vantec 500 area detector. The source radiation was Cu-K$_\alpha$ with the generator set at 40 kV and 40 mA, with a monochromated incident beam of diameter 0.8 mm. Data analysis was done using Bruker's software, LEPTOS v6.02. The traditional $\sin^2 \psi$-method was used to study the residual strain in the thin films [4, 8]. Atomic force microscopy (AFM) was used to study the film topographic properties.

3. Results and discussion

The XRD results obtained using the $\theta - 2\theta$ scanning mode are shown in Fig. 1(a). All the Cr reflections are

———————
*corresponding author; e-mail: alettap@uj.ac.za

seen for the film with $t = 452$ nm, while the sample with $t = 29$ nm the Cr (110) is more intense than the other peaks. It is for this reason the Cr (110) peak was used for the further residual strain and stress analysis in this paper. The inset in Fig. 1(a) shows the FWHM for the same peaks as function of t. This indicates a maximum value for the sample with $t = 80$ nm. Considering the Debye-Scherrer formula smaller grain size corresponds to a peak broadening associated with a higher FWHM [10], thus implying that the 80 nm sample should have smaller grains than the other films in this series. Figure 1(b) depicts the Cr (310) 2θ Bragg peak measured at different tilt angles ψ for the 452 nm sample. This peak is shown as a representative example to clearly depict the shift to lower 2θ angles on increasing ψ, indicating an increase in tensile stress.
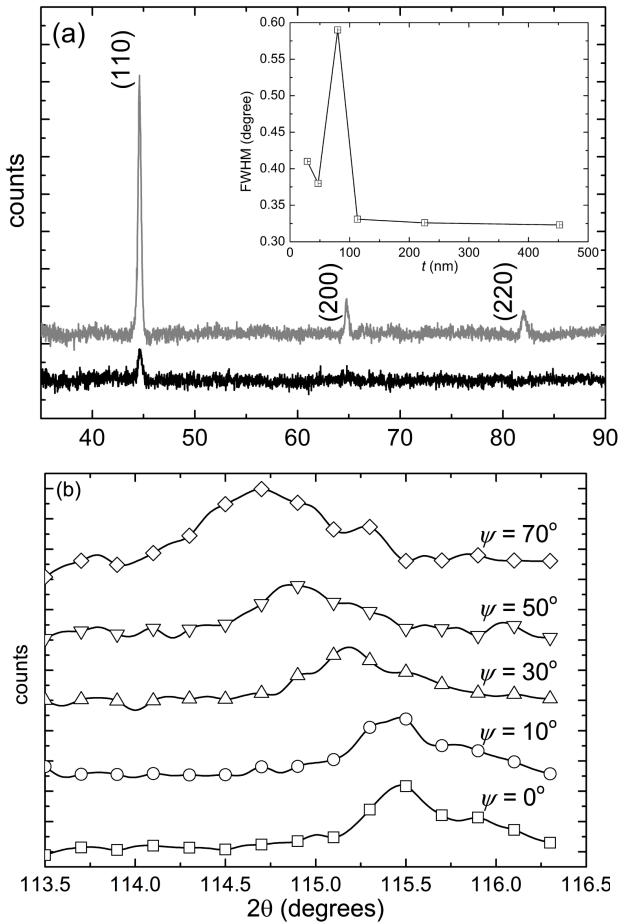

Fig. 1. (a) $\theta-2\theta$ XRD scans for Cr films with thickness $t = 452$ nm (grey) and 29 nm (black). The inset shows the FWHM for to each Cr (110) peak as function of t. (b) The Cr (310) 2θ Bragg peak for different tilt angles, ψ, measured on the 452 nm sample.

AFM images for samples with $t = 47$ nm and 80 nm are shown in Fig. 2(a) and (b), respectively. Although there is a variation in the grain sizes seen in each image, it is evident that the average grain size in the 80 nm sample are markedly smaller than that seen for the 47 nm
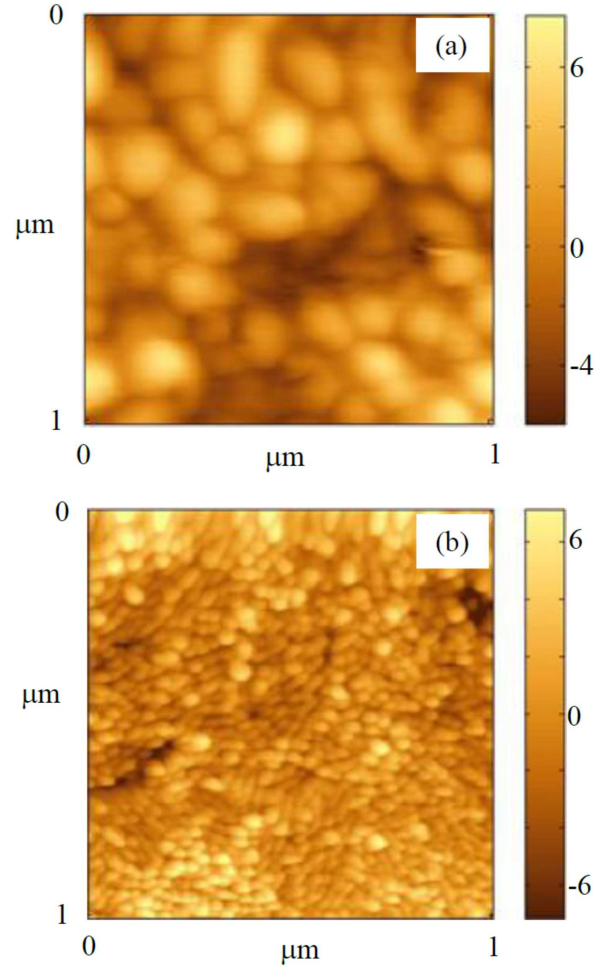

Fig. 2. AFM images for the $Cr_{99}Al_1$ samples with thicknesses (a) $t = 47$ nm and (b) $t = 80$ nm.

sample. This is in correspondence to what is expected from the XRD results. The average grain sizes seen in the other samples are comparable with those seen in for the $t = 47$ nm sample.

AFM and XRD results indicate that the films are textured polycrystalline. The degree of texture is subjected to an evolution during film growth [11] and pronounced textures are only obtained after certain layer thickness is achieved.

TABLE I

Principal stress components σ_{11} and σ_{22} obtained for $Cr_{99}Al_1$ thin films of thicknesses 29 nm to 452 nm.

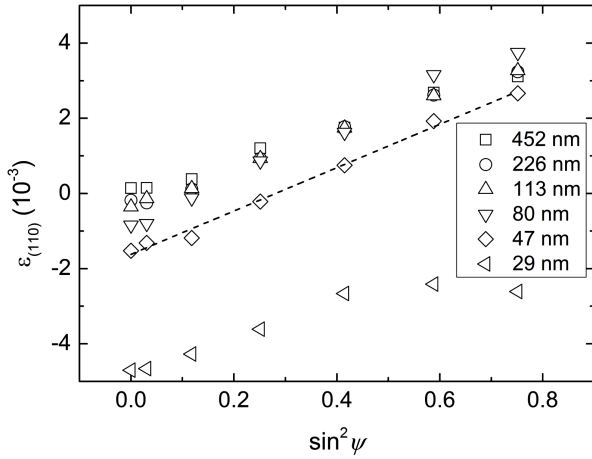| Thickness [nm]	Stress tensors [MPa]	
	σ_{11}	σ_{22}
29	833±54	827±54
47	1353±56	1390±56
80	1471±68	1430±68
113	1263±59	1207±59
226	1132±53	1089±53
452	925±50	908±50

Fig. 3. Plots of strain, $\varepsilon_{(110)}$, as function of $\sin^2 \psi$ for the different $Cr_{99}Al_1$ samples of various thicknesses. The broken line shows a linear fit to the data for the 47 nm thin film.

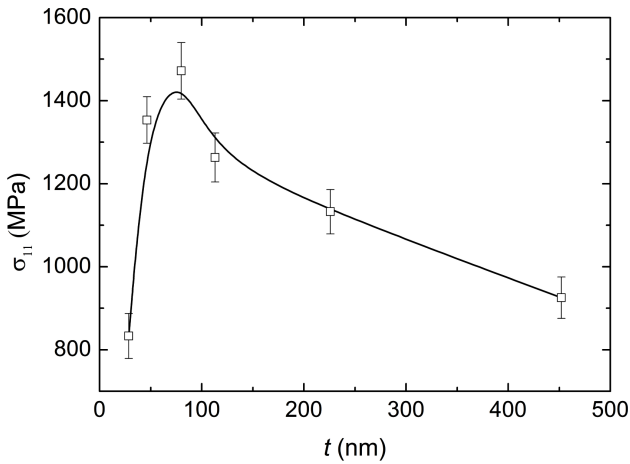Fig. 4. Residual stress (σ_{11}) as function of thin film thicknesses t for the $Cr_{99}Al_1$ thin films prepared on fused silica substrates. The solid line is a guide to the eye.

In Fig. 3 the strain, $\varepsilon_{(110)}$, as function of $\sin^2 \psi$ is shown for the $Cr_{99}Al_1$ layers with $29 \leqslant t \leqslant 452$ nm. The positive slopes in the $\varepsilon_{(110)}$ as function of $\sin^2 \psi$ plots indicate that the residual stress in the films are tensile [8]. The broken line shows, as a representative example, a linear fit of the form $\varepsilon_{(110)} = (0.0058 \pm 0.0002) \sin^2 - (0.00162 \pm 0.00009)$ to the $\varepsilon_{(110)} = \frac{d_{\phi\psi} - d_0}{d_0}$ as a function of $\sin^2 \psi$ data for the 47 nm thin film.

Considering the expression for the strain [4, 7]:

$$\varepsilon_{\varphi\psi} = \left(\frac{1+\nu}{E}\right)\sin^2 \psi - \left(\frac{\nu}{E}\right)(\sigma_{11} + \sigma_{22}), \qquad (1)$$

where σ_{φ} is the stress in the surface, E is the Young modulus, ν is the Poisson ratio, while σ_{11} and σ_{22} are the principal stress components. Assuming that $\sin^2 \psi = 0$ at the intercept, the unstrained lattice spacing d_0 can

then be obtained from:

$$d_{\phi 0} = d_0 - \left(\frac{\nu}{E}\right)_{110} d_0(\sigma_{11} + \sigma_{22}), \qquad (2)$$

where the slope of the plot is given by:

$$\frac{\partial d_{\phi\psi}}{\partial \sin^2 \psi} = \left(\frac{1+\nu}{E}\right)_{110}\sigma_\phi d_0. \qquad (3)$$

Residual stress components σ_{11} and σ_{22} were calculated using equations (2) and (3). These are shown in Table I. Figure 4 shows a plot of the σ_{11}-stresses as function of $Cr_{99}Al_1$ film thickness. A stress value of 833 MPa for the $t = 29$ nm film is obtained. With increasing thickness the stress increases to 1471 MPa for the $t = 80$ nm film, where after it gradually decreases with increase in t reaching a value of 925 MPa for the 452 nm film. The magnitude of the stress values obtained compare well with those obtained for pure polycrystalline Cr thin films [8], but the behaviour of $\sigma_{11}(t)$ differs in the two sample series. For the pure Cr thin films prepared on fused silica a minimum is observed in the $\sigma_{11}(t)$ curve for the 80 nm sample. The stress values for both the Cr and $Cr_{99}Al_1$ series reaches approximately 1100 MPa for samples with $t \approx 300$ nm.

The coefficient of thermal expansion (CTE) of Cr and $Cr_{99}Al_1$ is larger than that of fused silica substrate and these coatings will contract more than the substrate when the system is cooled from the deposition temperature. In addition the volume of substrate material present is substantially larger, causing tensile thermal stress [4, 8] in the thin coatings. Grain growth during film deposition also causes a tensile component of the intrinsic stress and can lead to the scaling of the stress with the inverse of the grain size [12]. It should also be taken into account that in the $Cr_{99}Al_1$ series the Al acts as an impurity in the Cr matrix that can result in smaller grain sizes and less mobile grain boundaries [13]. Figure 4 thus indicates that the $\sigma_{11}(t)$ behaviour is influenced by a variety of factors in competing mechanisms and that the grain size effect appears dominant for 80 nm sample that show the highest stress value.

4. Conclusions

The XRD results obtained using the $\theta - 2\theta$ scanning mode show that the $Cr_{99}Al_1$ thin films prepared on fused silica substrates are polycrystalline textured. The FWHM for the (110) peak as function of t indicates a maximum value for the sample with $t = 80$ nm implying small grains in this sample. This is confirmed considering the AFM results.

The residual strain and stress analysis of the $Cr_{99}Al_1$ thin films prepared on fused silica substrates, with thickness t varying from 29 nm to 452 nm, was done using the XRD $\sin^2 \psi$-technique. The stresses remain tensile regardless of the film thickness. It shows a stress value of 833 MPa for the $t = 29$ nm film. With increasing thickness the stress increases to 1471 MPa for the $t = 80$ nm film, where after it gradually decreases with increase in t to a value of 925 MPa for the 452 nm film. The $\sigma_{11}(t)$ behaviour is influenced by a variety of factors and competing mechanisms, but it is evident that for the $t = 80$ nm

sample, with the smallest average grain size, the highest stress value is obtained.

The effect of the differences in the coefficient of thermal expansion between the coatings and substrates, the Al doping in the Cr matrix, growth mechanisms and morphologies associated with the various thicknesses, as well as grain sizes should be taken into account to setting up a model to explain the complex $\sigma_{11}(t)$ curve obtained for the $Cr_{99}Al_1$ film series.

Acknowledgement

References

[1] E. Fawcett, H.L. Alberts, V.Y. Galkin, D.R. Noakes, J.V. Yakhmi, *Rev. Mod. Phys.* **66**, 25 (1994).

[2] H. Zabel, *J. Phys. Condens. Matter* **11**, 9303 (1999).

[3] Z.P. Mudau, A.R.E. Prinsloo, C.J. Sheppard, A.M. Venter, E.E. Fullerton, *SAIP Conf. Preceedings 2015*, 73.

[4] I.C. Noyan, T.C. Huang, B.R. York, *Crit. Rev. Solid State Mater.* **20**, 125 (1995).

[5] M.F. Doerner, S. Brennan, *J. Appl. Phys.* **63**, 126 (1998).

[6] J. Lu, *Handbook of measurement of residual stress*, Society for Experimental Mechanics Inc., Ed., The Fairmont Press Inc., 1995.

[7] B.D. Cullity, *Elements of X-ray Diffraction*, Addison Wesley, Reading, Massachusetts 1978.

[8] Z.P. Mudau, A.R.E. Prinsloo, C.J. Sheppard, A.M. Venter, E.E. Fullerton, *SAIP Conf. Preceedings 2014*, 34.

[9] S.Y. Chiou, B.H. Hwang, *J. Phys. D: Appl. Phys.* **31**, 349 (1998).

[10] J.I. Langford, A.J.C. Wilson, *J. Appl. Cryst.* **11**, 102 (1978).

[11] F. Fenske, B. Selle, M. Birkholz, *Jap. J. Appl. Phys. Lett.* **44**, L662 (2005).

[12] H.Z. Hang, C.V. Thompson, *Acta Materialia* **67**, 189 (2014).

[13] M. Adamik, P.B. Barna, I. Tomov, *Thin Solid Films* **359**, 33 (2000).